Spatial-Frequency 3D Fluorescence for Surgical Guidance: Margin Thickness Quantification

Hikaru Kurosawa[1], Natalie J. Won[1], Mandolin Bartling[2], Elise Schwarz[1], Matthew Siracusa[1], Brian C. Wilson[1,3], Jonathan C. Irish[1,2], Michael J. Daly[1]
[1]Princess Margaret Cancer Centre, University Health Network, Toronto, Canada
[2]Department of Otolaryngology-Head and Neck Surgery, University of Toronto, Toronto, Canada
[3]Department of Medical Biophysics, University of Toronto, Toronto, Canada

ABSTRACT

Accurate assessment of 3D surgical margins remains a challenge after tumor resection. Fluorescence-guided surgery systems show promise to provide precise identification of residual tumor on the surface of resected tissue, but existing 2D fluorescence imaging systems lack the ability to quantify the 3D margin (i.e., thickness of healthy tissue surrounding the resected tumor). In oral cancer, a 5 mm pathologic margin has been identified as the prognostic cutoff by several studies, indicating the clinical significance of assessing subsurface information in tissue. To quantify the 3D surgical margins in *ex vivo* surgical specimens, our group has been developing a deep learning (DL)-enabled 3D fluorescence spatial frequency domain imaging (SFDI) system. Here, we examine the utility of *in silico* training for margin thickness quantification. A set of 10,000 synthetic tumors were generated using composite spherical harmonics (CSH) and passed into a diffusion theory light propagation model to output fluorescence and reflectance images. Optical property maps were subsequently extracted using a lookup table. The fluorescence images and optical property maps were input into a custom Siamese attention U-net to predict fluorophore concentration and subsurface depth. DL performance was evaluated using *in silico* testing data of: i) CSH; and ii) patient-derived oral cancer tumor shapes. Analysis included the overall depth and concentration error as well as the classification metrics for determining margin status. Future studies are required to assess DL performance in phantom and animal experiments.

Keywords: Fluorescence-guided surgery, spatial frequency domain imaging, structured illumination, oral cancer surgery, surgical margins, deep learning, optical reconstruction

1. INTRODUCTION

Tumor delineation remains a significant challenge in oral cancer surgery.[1] With most oral cancer patients requiring surgical intervention as part of treatment, accurate assessment of tumor margins is critical for complete resection of tumor while maximizing preservation of healthy tissue.[2] To determine the borders of tumors, various intraoperative techniques including palpation, visual cues, pathology, and anatomical imaging are applied;[3] however, they are limited in precision, resulting in a positive margin incidence in oral cancer as high as 85%.[4]

Fluorescence-guided surgery is an emerging intraoperative imaging modality that has been investigated to improve cancer surgery outcomes.[5] This technique utilizes fluorescence contrast agents and fluorophore-specific wavelengths of light to enable absorption and subsequent emission of light at a longer wavelength, amplifying the tumor-tissue contrast.[6]

While fluorescence-guided surgery shows promise in tumor delineation, traditional 2D fluorescence optical devices are limited to only provide lateral margin information, restricting its application primarily for assessment of tissue information on the residual surface.[7] To address this limitation, our group has been developing a spatial frequency domain imaging (SFDI) approach for fluorescence tomography to quantify subsurface depth. Briefly, SFDI projects structured light at different spatial frequencies to capture reflectance or fluorescence images,[8] with higher spatial frequencies more sensitive to tissue blurring than the lower frequencies, which enables depth sampling within tissue.[9]

Obtaining depth-resolved fluorescence for tumor delineation may prove beneficial for two clinical scenarios in oral cancer surgery. The first case is when oral cancer is present on the mucosal surface and infiltrates deeper into healthy tissue. This "iceberg" configuration is shown in Figure 1a, which would be encountered during *in vivo* imaging of the

Molecular-Guided Surgery: Molecules, Devices, and Applications XI, edited by Summer L. Gibbs, Kenneth M. Tichauer, Proc. of SPIE Vol. 13301, 1330102 · © 2025 SPIE
1605-7422 · doi: 10.1117/12.3042275

oral cancer before resection. The second case is when the "iceberg" oral cancer tumor is resected (i.e. *ex vivo*) and flipped upside down to assess the margin (healthy tissue) thickness. Figure 1b shows a tumor that is buried below healthy tissue that we will refer to as the "submarine" model.

For "submarine" tumors, pathology analysis of the resected tumor is conducted to measure the margin thickness and determine its status.[10] For oral cancer, the prognostic cutoff is commonly defined to be 5 mm, classifying a margin thickness below and above 5 mm as positive and negative margin, respectively.[2,11] Although histopathology has been the standard method for determining margin status, it often takes several days to present the definitive status.[10] A method to provide faster feedback on margin status is critical to improve surgery efficiency and outcomes.

Previous work by our group has demonstrated proof-of-concept using an *in silico* trained deep learning (DL) 3D fluorescence SFDI system to accurately predict depths of an "iceberg" tumor model.[12] Here, we extend upon that study by applying the DL-enabled SFDI technology to the "submarine" problem. Several studies have explored the depth quantification of buried objects using various fluorescence imaging techniques;[13–19] however, they are limited in depths, optical property ranges, and diversity in tumor shapes that were considered. This simulation study examines the utility of *in silico* training to quantify margin thickness on complex tumor shapes derived from pre-operative MRI images of tongue cancer patients.

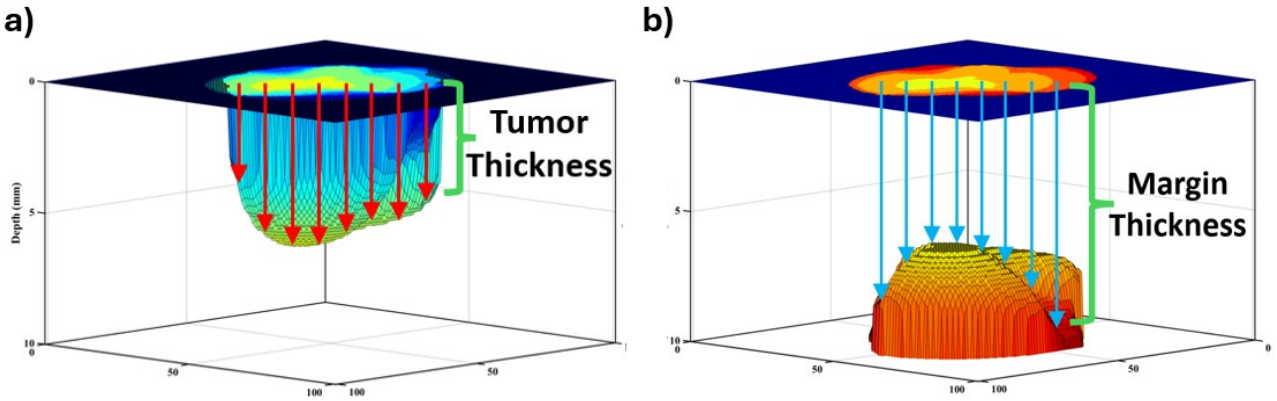

Figure 1: 3D model of synthetic tumor shapes. (a) "iceberg" tumor found at the tissue surface and (b) "submarine" tumor buried inside healthy tissue

2. METHODS

2.1 Deep Learning Architecture

A suitable model to predict the subsurface depth and concentration of a buried object is explored. Previous studies from our group have demonstrated viability of a Siamese convolutional neural network (CNN) architecture that utilizes optical properties and spatial frequency domain fluorescence images as the inputs in predicting the bottom surface and fluorophore concentration of a buried object ("iceberg").[12] This work was adapted from research conducted by Smith et al in predicting the subsurface depth ("submarine") using optical properties and macroscopic fluorescence lifetime images as inputs.[19] Here, we extend upon those studies and adopt the Siamese attention U-net architecture as shown in Figure 2, retaining the two branch two output structures while modifying the intermediate steps that follow the concatenation of the two branches (31,778,949 parameters).[20] After concatenation of the two branches, it undergoes an encoder-decoder structure to allow extraction of image features at different image scales.[21] The long skip connections from the encoder path are passed through the attention gates to disregard irrelevant information.[20] After the decoder path, the layer is branched to output the concentration and depth maps of the buried object. This architecture modification was made to support deeper learning by extracting context information and output high resolution prediction maps.

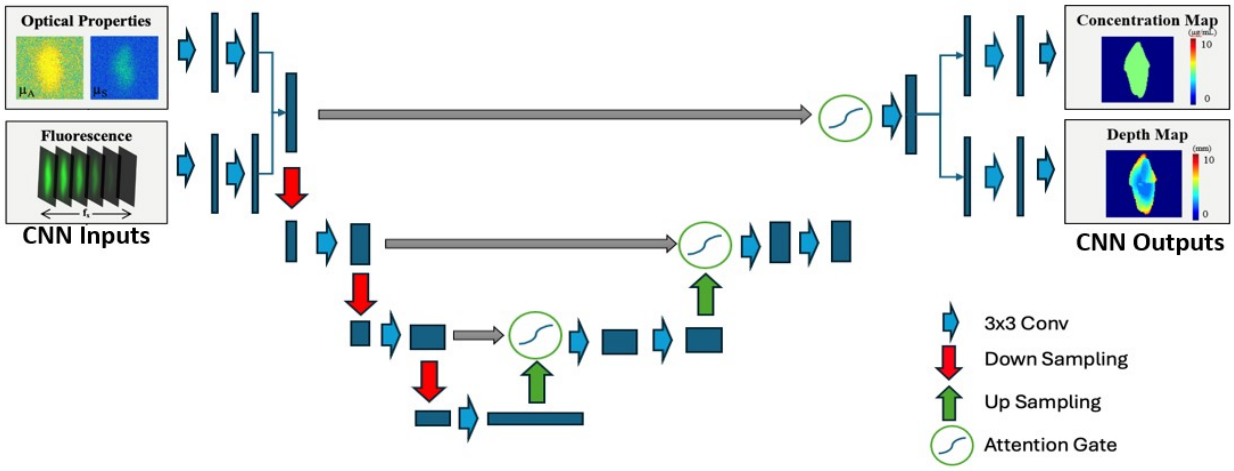

Figure 2: Siamese attention U-net DL architecture with optical property maps and spatial frequency domain fluorescence images as inputs to predict concentration and depth maps of the buried fluorescent object

2.2 Deep Learning Training

DL training requires a large volume of data. Our previous study demonstrated the utility of *in silico* training in producing accurate DL results using an in-house numerical diffusion theory light propagation model.[12] Here, 10,000 synthetic tumor shapes using composite spherical harmonics were generated in MATLAB. Composite spherical harmonics (CSH) were created by merging four spherical harmonics with random order and degree = 2 to 6, width = 5 to 40 mm, height = 5 to 10 mm, and minimum top surface depth = 1 to 10 mm. The generated shapes were passed into the SFDI simulation system to produce synthetic reflectance and fluorescence images (101 × 101 pixels, 0.5 mm / pixel) across 6 spatial frequencies (f_x = [0, 0.05, 0.1, 0.15, 0.2, 0.25] mm^{-1}) (~1 h simulation time). Reflectance images were further processed to estimate the absorption and scattering coefficient maps using an SFDI lookup table computed at two separate spatial frequencies f_x = [0 and 0.2] mm^{-1}. The training set were generated for an excitation wavelength of 630 nm by randomly assigning a homogeneous optical property across the entire tissue, with absorption μ_a values between 0.0015 to 0.015 mm^{-1}, scattering μ_s of 0.75 to 2 mm^{-1} and PpIX fluorophore concentration between 1 to 10 µg/ml for each tumor case. Additionally, a randomized amount of fluorescence was added to the healthy tissue background of 0.1% to 50% of the fluorescence concentration of the tumor. Those data were input into the DL model on Amazon Web Services (AWS) SageMaker with ml.g5.2xlarge instance type (1 NVIDIA A10G GPU, 8 vCPU) for ~2 hour training time. A depth of 10 mm was assigned to all points in the background to have the minimum distance in the depth map be the tumor body instead of the healthy tissue.

2.3 Deep Learning Testing

The model performance was tested using *in silico* testing data. 1000 CSH were newly generated with the same shape parameter ranges (order, degree, width, height, minimum depth) as the training set. The testing cases had fixed optical properties (μ_a = 0.0045 mm^{-1}, μ_s = 1 mm^{-1}), fluorophore concentration (5 µg/ml), and randomized healthy tissue fluorescence = 0.1 % to 50% of tumor fluorophore concentration. Those optical property values fell within the nominal ranges for both healthy oral tissue and cancer.[22] The mean absolute error (MAE) and standard deviation (SD) between the predicted and ground truth values of the depth map and concentration maps were computed. The depth map was further used to predict the minimum margin thickness (minimum depth) and classify the margin as clear (0) or positive (1) using a cutoff of 5 mm.

To evaluate DL capacity to make predictions for tumor shapes with more complex features seen in real tumors, patient-derived oral cancer tumor meshes were extracted by contouring preoperative MRI of tongue cancer patients as displayed in Figure 3a. This was performed under institutional ethics board approval for retrospective patient data access (University Health Network REB #22-5471). Using the 20 patient-derived data, the bottom surface (region with healthy tissue) was oriented upwards, and the minimum margin thickness was set to 1-10 mm in 1 mm increments as shown in Figure 3c. These transformations resulted in a total of 200 patient-derived tumors.

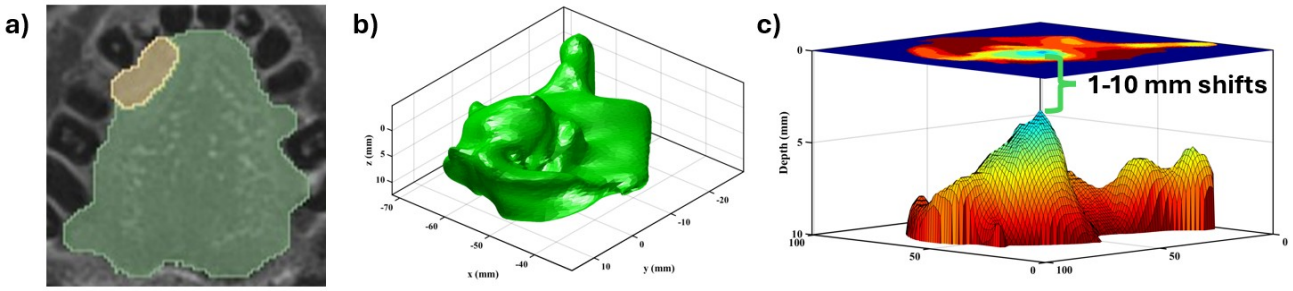

Figure 3: Patient-derived tongue tumors are used as test data. (a) Contoured MRI of the tongue tumor. (b) 3D plot of the contoured volume (c) Tumor shape buried inside healthy tissue with minimum margin thickness set to 1-10 mm.

3. RESULTS

The MAE (SD) of depth and concentration for the 1000 CSH were 0.47 (0.80) mm and 1.63 (1.25) µg/ml, respectively. The MAE of the minimum margin thickness was 0.23 (0.19) mm with classification accuracy, specificity, sensitivity, precision of 0.97, 0.96, 0.97, and 0.96, respectively. Figure 4a shows DL predictions for all points in representative CSH test cases and Figure 4b shows the minimum margin thickness graph with blue and red dots resembling correct and incorrect classifications, respectively.

The MAE of depth and concentration for the 200 patient-derived tumors were 1.56 (1.83) mm and 2.29 (1.57) µg/ml, respectively. The MAE of the minimum depth was 0.44 (0.32) mm with classification accuracy, specificity, sensitivity, precision of 0.97, 0.96, 0.99, and 0.94, respectively. Figure 5a shows the depth and concentration maps and Figure 5b shows the minimum depth graph.

Overall, the depth error had a four-fold increase from CSH to patient-derived tumors. This can be attributed to the greater topography irregularity present in patient tumors, displaying more fluctuations in depths across the entire surface. Additionally, some patient tumors exhibit protrusions up to 3 mm in height, as shown in Figure 6, which can lead to false negative cases when the protrusions are not sufficiently resolved. It is critical to note that while the overall depth and concentration error increased by 1.09 mm, the minimum margin thickness error increased only by 0.21 mm, maintaining the high classification accuracy. This demonstrates the strength of the DL model in predicting the minimum distance better than the rest of the points, indicating its potential utility for margin classification applications.

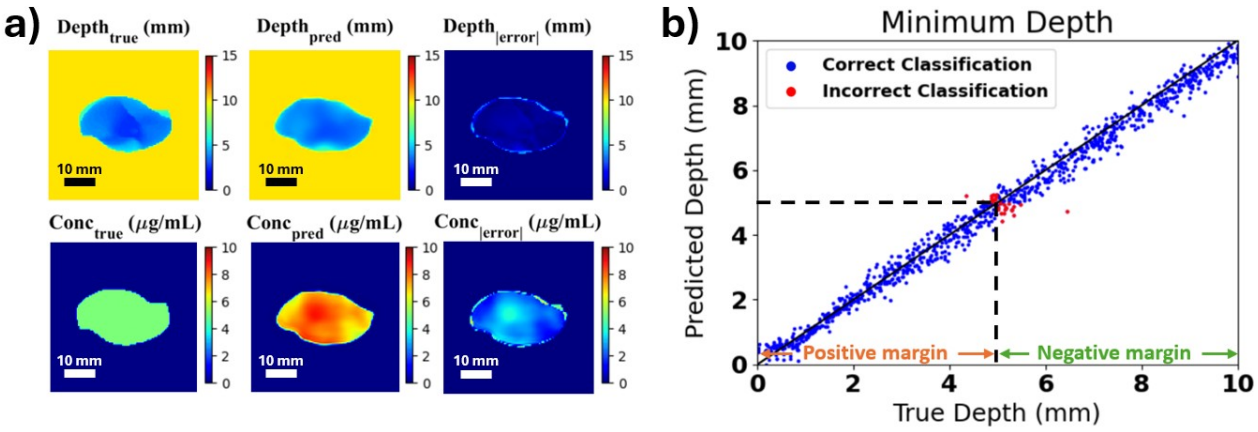

Figure 4: DL predictions for 1000 CSH test cases. (a) Depth and concentration predictions for representative CSH test cases. Ground truth depth and concentration maps are compared to the predicted outputs. (b) Minimum margin thickness graph for CSH test data. Cutoff value of 5 mm is used for positive (< 5 mm) and negative (> 5 mm) margin.

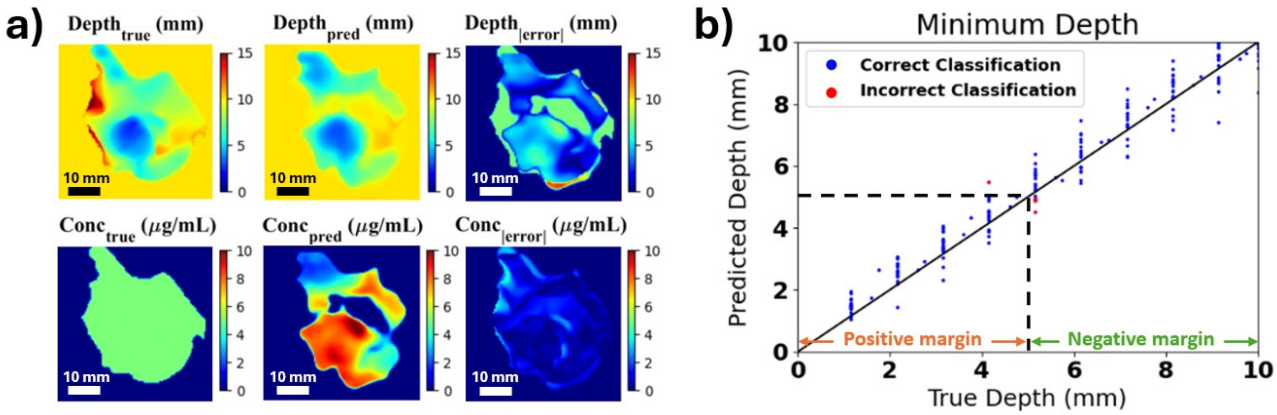

Figure 5: Same as Figure 4 for 200 patient-derived tumor shape test cases.

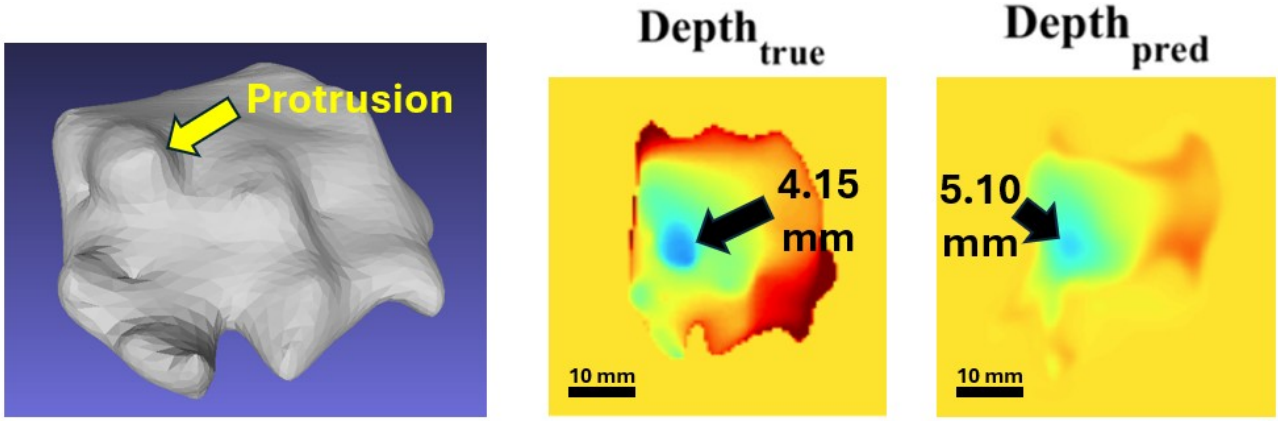

Figure 6: Example of a patient-derived tumor case with false negative classification. The prediction misclassified the margin as negative at the protrusion location. The depth color scale is the same as in Figure 5.

4. CONCLUSIONS AND FUTURE DIRECTIONS

This preliminary simulation study demonstrated the applicability of DL-enabled SFDI for margin thickness quantification and classification in complex tumor shapes. The overall depth error increased with increasing shape complexity, as prediction in patient cases became more challenging due to the higher irregularity across the surface. The presence of protrusions complicated the structural resolution, increasing the likelihood of misclassifications at those sites. Incorporation of those geometrical features seen in patient cases into training data may help improve accuracy in more complex tumor shapes. Still, the quality of minimum depth prediction and margin classification was promising for both CSH and patient-derived tumors, showing potential that motivates translation to future testing in real physical data.

Limitations of this simulation study include the assumption of a flat tissue surface and homogeneous optical properties and fluorophore distributions, and so future work is necessary to study the effects of surface topography and optical heterogeneities on performance. Furthermore, our study included a limited range of optical properties in the test cases (μ_a=0.0045 mm^{-1}, μ_s' = 1 mm^{-1}) to simulate typical ranges of both healthy oral tissue and cancer tumor properties, but those values can vary significantly in real patient cases.[22] Especially for absorption, this may be higher in conditions with higher vasculature at the tumor sites, which can limit the optical penetration depth and decrease the tumor to background contrast (i.e. image quality) of the extracted images, consequently decreasing performance. It is important to be aware that a combination of those parameters would define the conditions in which this approach can be reliably used.

Future testing will be conducted using phantom and animal preclinical oral cancer models to validate with a physical SFDI system. Testing in those more complex cases is essential to enable clinical translation of the system.

ACKNOWLEDGEMENTS

This work is supported by the Department of Otolaryngology – Head & Neck Surgery, University of Toronto (Raymond Ng & Wendy Chui Foundation for Innovation, Barberian Research Award, Artificial Intelligence (AI) Fund Award) and the Princess Margaret Cancer Foundation (Garron Family GTx Surgery – Engineering Fund, Allison Family GTx AI Engineering Scholarship Fund, Lucky Bean Foundation GTx STEM Research Scholarship Program).

REFERENCES

[1] Pagedar, N. A., "Better Visualization of Oral Cancer Margins-A Struggle of Cancer and Technology," JAMA Otolaryngol Head Neck Surg **146**(12), 1156–1157 (2020).

[2] Chen, T.-C., Wang, C.-P., Ko, J.-Y., Yang, T.-L. and Lou, P.-J., "The impact of pathologic close margin on the survival of patients with early stage oral squamous cell carcinoma.," Oral Oncol **48**(7), 623–628 (2012).

[3] Luryi, A. L., Chen, M. M., Mehra, S., Roman, S. A., Sosa, J. A. and Judson, B. L., "Positive surgical margins in early stage oral cavity cancer: an analysis of 20,602 cases.," Otolaryngol Head Neck Surg **151**(6), 984–990 (2014).

[4] Smits, R. W. H., Koljenović, S., Hardillo, J. A., Ten Hove, I., Meeuwis, C. A., Sewnaik, A., Dronkers, E. A. C., Bakker Schut, T. C., Langeveld, T. P. M., Molenaar, J., Hegt, V. N., Puppels, G. J. and Baatenburg de Jong, R. J., "Resection margins in oral cancer surgery: Room for improvement," Head Neck **38 Suppl 1**, E2197-2203 (2016).

[5] Vahrmeijer, A. L., Hutteman, M., van der Vorst, J. R., van de Velde, C. J. and Frangioni, J. V., "Image-guided cancer surgery using near-infrared fluorescence," Nat Rev Clin Oncol **10**(9), 507–518 (2013).

[6] Keereweer, S., Van Driel, P. B., Snoeks, T. J., Kerrebijn, J. D., Baatenburg de Jong, R. J., Vahrmeijer, A. L., Sterenborg, H. J. and Lowik, C. W., "Optical image-guided cancer surgery: challenges and limitations," Clin Cancer Res **19**(14), 3745–3754 (2013).

[7] Pogue, B. W., Rosenthal, E. L., Achilefu, S. and van Dam, G. M., "Perspective review of what is needed for molecular-specific fluorescence-guided surgery," J Biomed Opt **23**(10), 1–9 (2018).

[8] Cuccia, D. J., Bevilacqua, F., Durkin, A. J., Ayers, F. R. and Tromberg, B. J., "Quantitation and mapping of tissue optical properties using modulated imaging," J Biomed Opt **14**(2), 024012 (2009).

[9] Gioux, S., Mazhar, A. and Cuccia, D. J., "Spatial frequency domain imaging in 2019: principles, applications, and perspectives," Journal of Biomedical Optics **24**(7), 1–18 (2019).

[10] Brouwer de Koning, S. G., Schaeffers, A. W. M. A., Schats, W., van den Brekel, M. W. M., Ruers, T. J. M. and Karakullukcu, M. B., "Assessment of the deep resection margin during oral cancer surgery: A systematic review," Eur J Surg Oncol **47**(9), 2220–2232 (2021).

[11] Solomon, J., Hinther, A., Matthews, T. W., Nakoneshny, S. C., Hart, R., Dort, J. C. and Chandarana, S. P., "The impact of close surgical margins on recurrence in oral squamous cell carcinoma," J Otolaryngol Head Neck Surg **50**(1), 9 (2021).

[12] Won, N. J., Bartling, M., Macchia, J. L., Markevich, S., Holtshousen, S., Jagota, A., Negus, C., Najjar, E., Wilson, B. C., Irish, J. C. and Daly, M. J., "Deep learning–enabled fluorescence imaging for surgical guidance: in silico training for oral cancer depth quantification," J Biomed Opt **30**(S1), S13706 (2024).

[13] van Keulen, S., Nishio, N., Birkeland, A., Fakurnejad, S., Martin, B., Forouzanfar, T., Cunanan, K., Colevas, A. D., S. van den Berg N and Rosenthal, E., "The Sentinel Margin: Intraoperative Ex Vivo Specimen Mapping Using Relative Fluorescence Intensity," Clin Cancer Res **25**(15), 4656–4662 (2019).

[14] Krishnan, G., van den Berg, N. S., Nishio, N., Kapoor, S., Pei, J., Freeman, L., Lee, Y. J., Zhou, Q., van Keulen, S., Farkurnejad, S., Condon, J., Baik, F. M., Martin, B. A. and Rosenthal, E. L., "Fluorescent Molecular Imaging Can Improve Intraoperative Sentinel Margin Detection in Oral Squamous Cell Carcinoma," J Nucl Med **63**(8), 1162–1168 (2022).

[15] Kolste, K. K., Kanick, S. C., Valdes, P. A., Jermyn, M., Wilson, B. C., Roberts, D. W., Paulsen, K. D. and Leblond, F., "Macroscopic optical imaging technique for wide-field estimation of fluorescence depth in optically turbid media for application in brain tumor surgical guidance," J Biomed Opt **20**(2), 26002 (2015).

[16] Jermyn, M., Kolste, K., Pichette, J., Sheehy, G., Angulo-Rodriguez, L., Paulsen, K. D., Roberts, D. W., Wilson, B. C., Petrecca, K. and Leblond, F., "Macroscopic-imaging technique for subsurface quantification of near-infrared markers during surgery," J Biomed Opt **20**(3), 036014 (2015).

[17] Kim, A., Roy, M., Dadani, F. N. and Wilson, B. C., "Topographic mapping of subsurface fluorescent structures in tissue using multiwavelength excitation," J Biomed Opt **15**(6), 066026 (2010).
[18] Rounds, C. C., de Wit, J. G., Vonk, J., Vorjohan, J., Nelson, S., Trang, A., Villinski, B., Samkoe, K. S., Brankov, J. G., Voskuil, F. J., Witjes, M. J. H. and Tichauer, K. M., "Improved intraoperative identification of close margins in oral squamous cell carcinoma resections using a dual aperture fluorescence ratio approach: first in-human results.," J Biomed Opt **29**(1), 016003 (2024).
[19] Smith, J. T., Aguenounon, E., Gioux, S. and Intes, X., "Macroscopic fluorescence lifetime topography enhanced via spatial frequency domain imaging," Opt Lett **45**(15), 4232–4235 (2020).
[20] Oktay, O., Schlemper, J., Folgoc, L. L., Lee, M., Heinrich, M., Misawa, K., Mori, K., McDonagh, S., Hammerla, N. Y., Kainz, B., Glocker, B. and Rueckert, D., "Attention U-Net: Learning Where to Look for the Pancreas," arXiv:1804.03999 (2018).
[21] Ronneberger, O., Fischer, P. and Brox, T., "U-Net: Convolutional Networks for Biomedical Image Segmentation," arXiv:1505.04597 (2015).
[22] Hu, F., Vishwanath, K., Wolfgang Beumer, H., Puscas, L., Afshari, H. R., Esclamado, R. M., Scher, R., Fisher, S., Lo, J., Mulvey, C., Ramanujam, N. and Lee, W. T., "Assessment of the sensitivity and specificity of tissue-specific-based and anatomical-based optical biomarkers for rapid detection of human head and neck squamous cell carcinoma," Oral Oncology **50**(9), 848–856 (2014).